Supporting Information

Oxidation of Methane to Methanol over Pd@Pt Nanoparticles under Mild Conditions in Water

Jianjun Chen [a,b,†], Sikai Wang [a,c,†], Laurent Peres[c], Vincent Collière[d], Karine Philippot[c], Pierre Lecante[d], Yaoqiang Chen[b]*, Ning Yan[a]*

[a] Department of Chemical and Biomolecular, National University of Singapore, 4 Engineering Drive, Singpore 117585, Singapore, E-mail: ning.yan@nus.edu.sg

[b] Institute of New Energy and Low-carbon Technology, Sichuan University, Chengdu 610064, China, E-mail: chenyaoqiang@scu.edu.cn

[c] Joint School of National University of Singapore and Tianjin University, International Campus of Tianjin University, Binhai New City, Fuzhou 350207, China.

[d] CNRS, LCC (Laboratoire de Chimie de Coordination), 205 route de Narbonne, BP44099, F-31077 Toulouse Cedex 4, France.

[e] *.CNRS, CEMES (Centre d'Élaboration des Matériaux et d'Études Structurales), 29 Rue Jeanne-Marvig, BP 4347, F-31055 Toulouse Cedex 4, France.*

† These authors contributed equally to this work

Table S1. Blank reactions performed in order to attest of the carbon source

Entry	Samples	CH_4 pressure (bar)	Products(μmol)				
			CH_3OOH	CH_3OH	HCHO	HCOOH	CO_2
1	PVP	0	0	0	0	0	-
2	PVP	30	0	0	0	0	-
3	Pd@Pt-PVP	0	0	0	0	0	-
4	Pd@Pt-PVP	30	4.4	2.3	0.3	0	0.3

Reaction conditions: 400 μmol H_2O_2, 50 °C for 0.5 h, 800 rpm

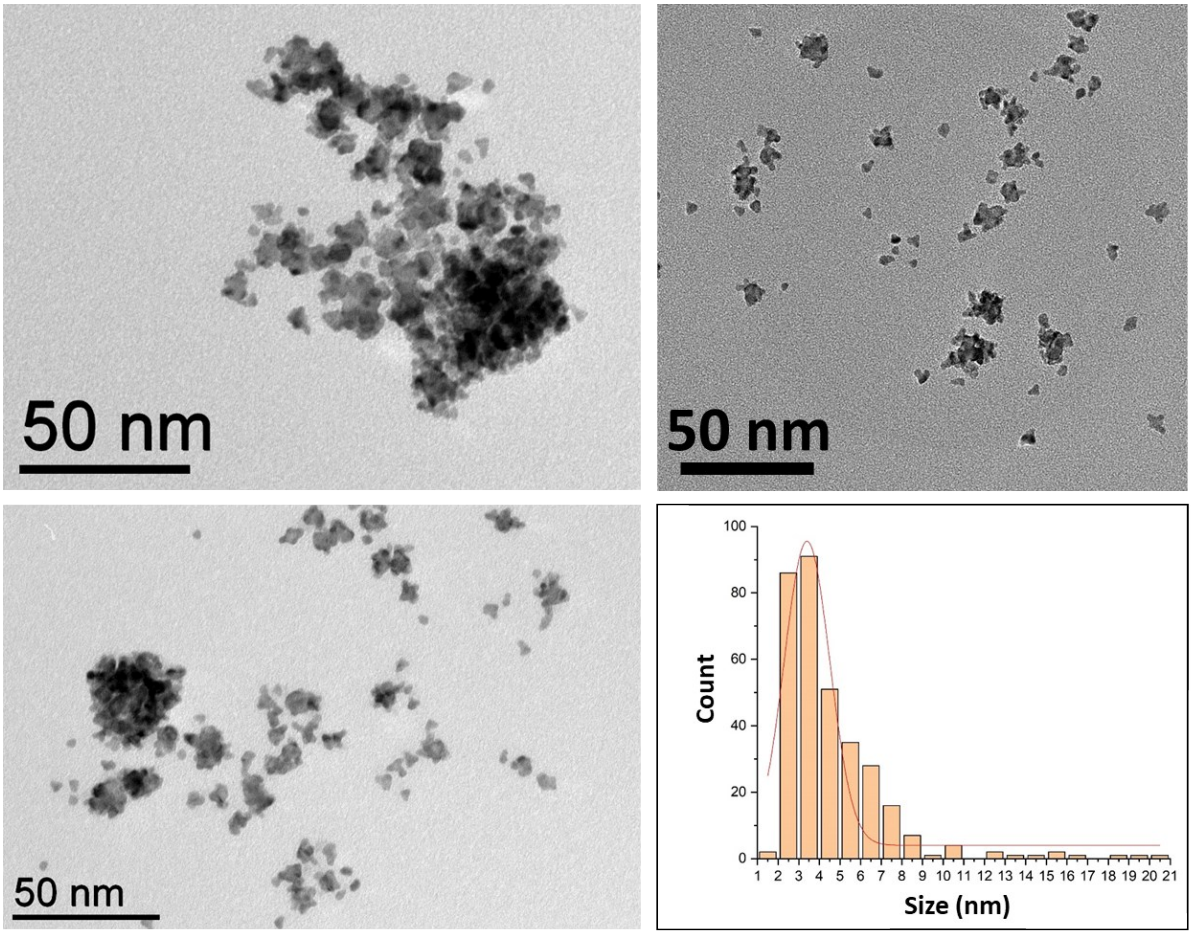

Figure S1. TEM images and size distribution of Pd@Pt NPs (mean size= 3.4 ± 2.2nm).

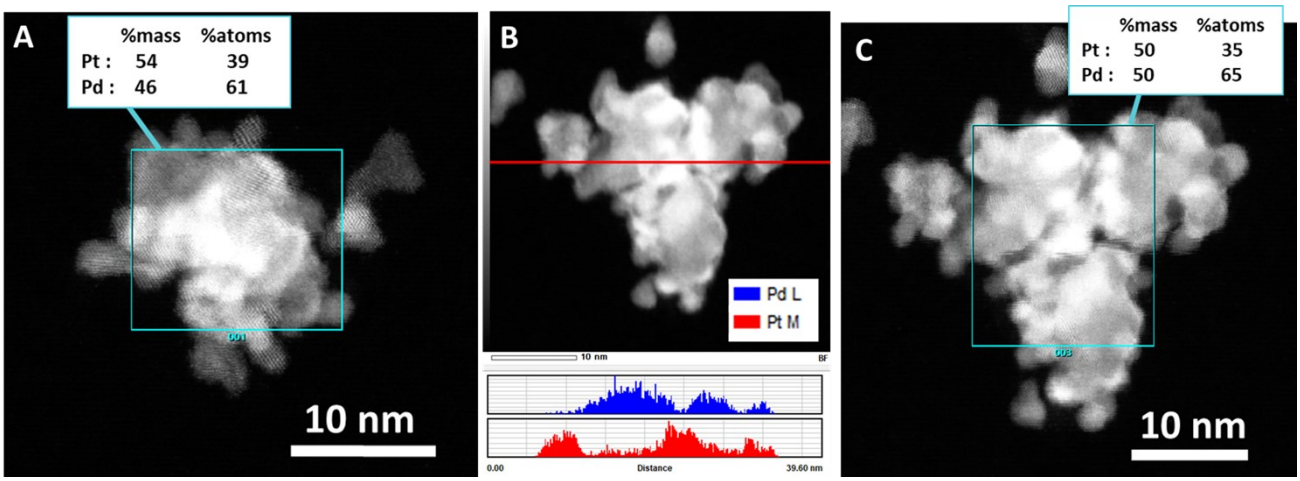

Figure S2: A. and C. STEM-EDX elemental analysis of aggregates of NPs with the corresponding elemental Pd and Pt compositions, and B. STEM-EDX line analysis of the aggregate presented in A., with the Pd (blue) and Pt (red) distribution along the line.

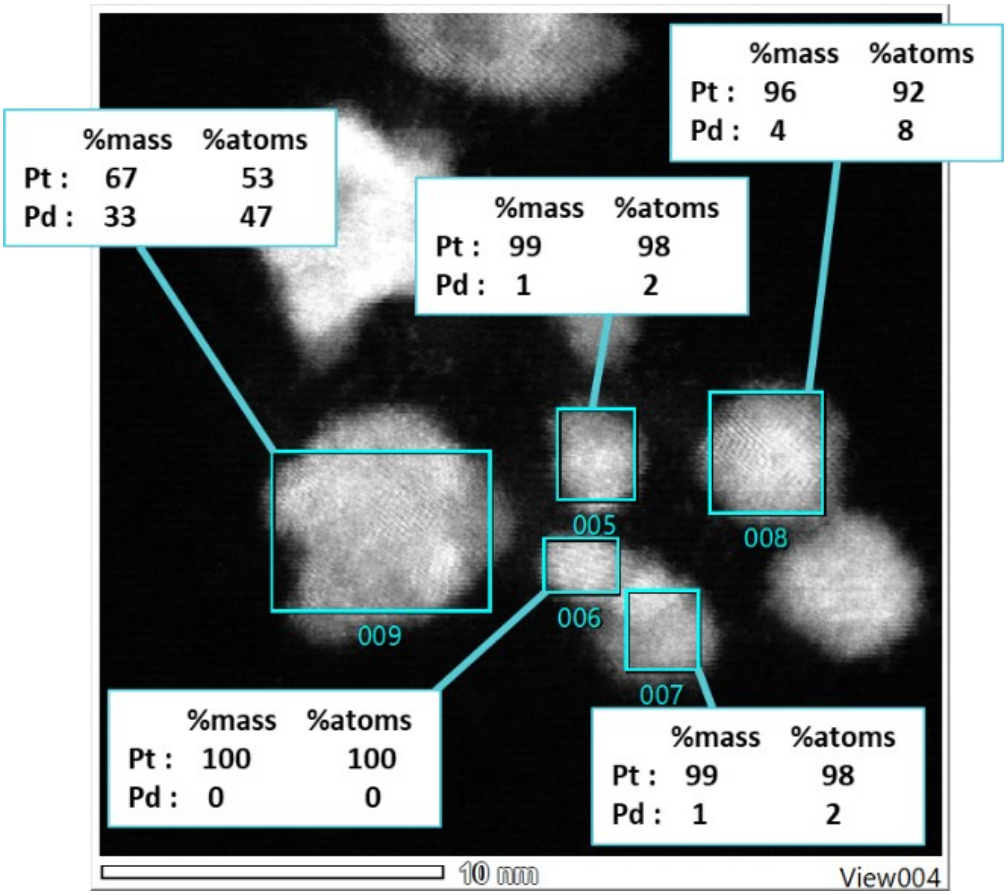

Figure S3: STEM-EDX elemental analysis of different type of particles, with the elemental Pd and Pt composition.

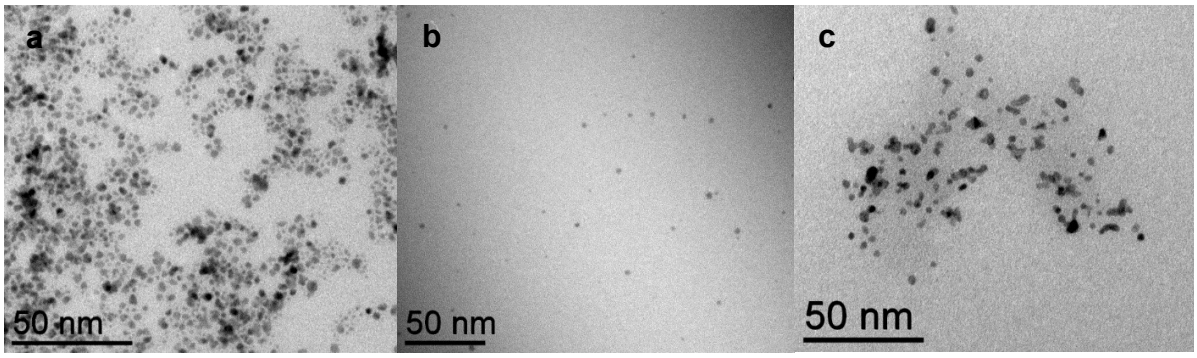

Figure S4. TEM images of Pt, Pd and PtPd(molar ratio=1:1) colloid nanoparticles. The mean sizes of the particles are 2.1±1.3, 2.1±1.5 and 2.7±1.2 nm, respectively.

The core-shell Pd@Pt structure presents larger size (smaller specific surface area) than those of Pt, Pd and PdPt particles, while the productivity and primary oxygenate selectivity are larger. Thus, Pd@Pt should have better methane oxidation activity.

To quantify the inherent activity, turnover frequency (TOF) was further calculated by the following equation. The amount of surface metal elements is calculated from the average particle sizes observed by TEM (Figure S1). The results are listed in Table S2.

$$TOF = \frac{n_{oxygenate}}{n_{surface\ metal} t}$$

Table S2. Total oxygenate productivity and turnover frequency of Pd, Pt, Pd@Pt and PdPt nano colloid samples

	Total oxygenate productivity ($mol_{oxygenate}\ mol_{metal}^{-1}$)	TOF ($mol_{oxygenate}\ mol_{surf\ metal}^{-1}\ h^{-1}$)
Pt	1.5	5.7
Pd	4.5	17.0
Pd@Pt	7	34.0
PdPt	5.1	19.4

Table S3. Liquid-phase methane oxidation performance of other reported heterogeneous catalysts

	Temp. (℃)	Oxidants	Methanol Sel.	Primary oxygenate prod.	Source
Pd@Pt colloids	50	H_2O_2	92.4%	89.3 mol $kg_{Pd@Pt}^{-1}$ h^{-1}	This work
AuPd/ZSM-5-R	70	O_2	92%	91.6 mol kg_{AuPd}^{-1} h^{-1}	1
Au-Pd colloids	60	H_2O_2	58%	43.4 mol kg_{AuPd}^{-1} h^{-1}	2
0.13AuPd/TiO_2	50	H_2O_2	90.7%	0.614 mol kg_{cat}^{-1} h^{-1}	3
0.3Rh/ZrO2	70	H_2O_2	74%	12.4 mol kg_{Rh}^{-1} h^{-1} 0.037 mol kg_{cat}^{-1} h^{-1}	4
0.6Rh/TiO2	150	CO and O_2	100%	76.7 mol kg_{cat}^{-1} h^{-1}	5
SAs Rh-CeO2 NWs (0.13 wt%)	50	H_2O_2	93.9%	3.7 mol kg_{cat}^{-1} h^{-1}	6
Cr_1/TiO_2	50	H_2O_2	48%	2.09 mol kg_{cat}^{-1} h^{-1}	7
Fe-MFI zeolite	50	H_2O_2	85%	9.50 mol kg_{cat}^{-1} h^{-1}	8
$Pd_xCu_{1-x}O/C$	50	H_2O_2	93.9%	4.08 mol kg_{cat}^{-1} h^{-1}	9
FeN_4/GN	25	H_2O_2	41%	3.44 mol kg_{Fe}^{-1} h^{-1} 0.093 mol kg_{cat}^{-1} h^{-1}	10

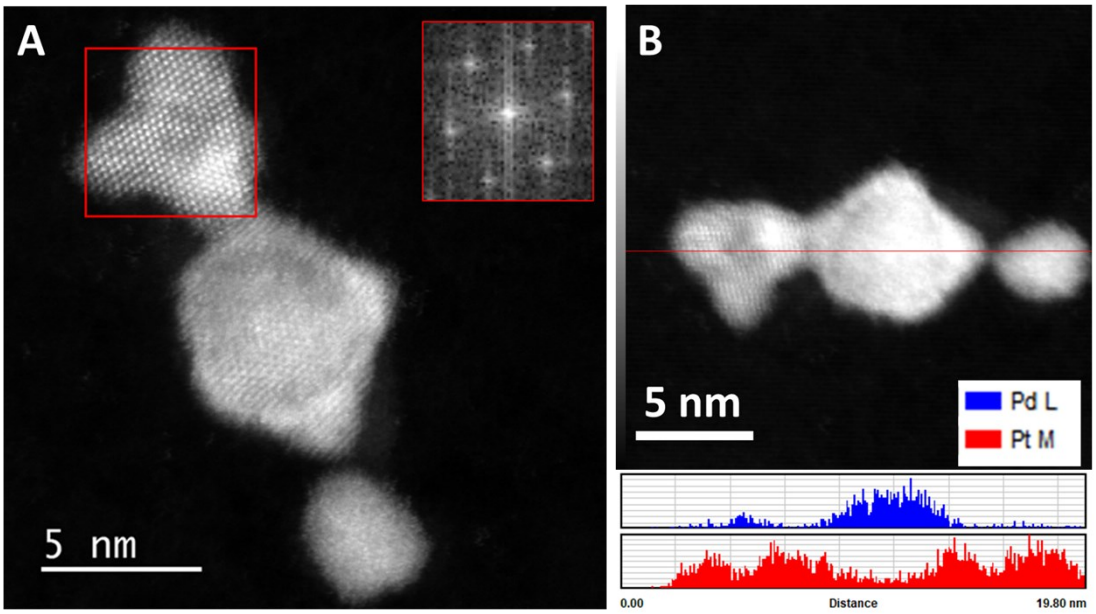

Figure S5: A. STEM-HREM dark field image of Pd@Pt NPs with the Fourier transform of the square red area in the inset and B. STEM-EDX line analysis of the same nanoparticles with the Pd (blue) and Pt (red) distribution along the line.

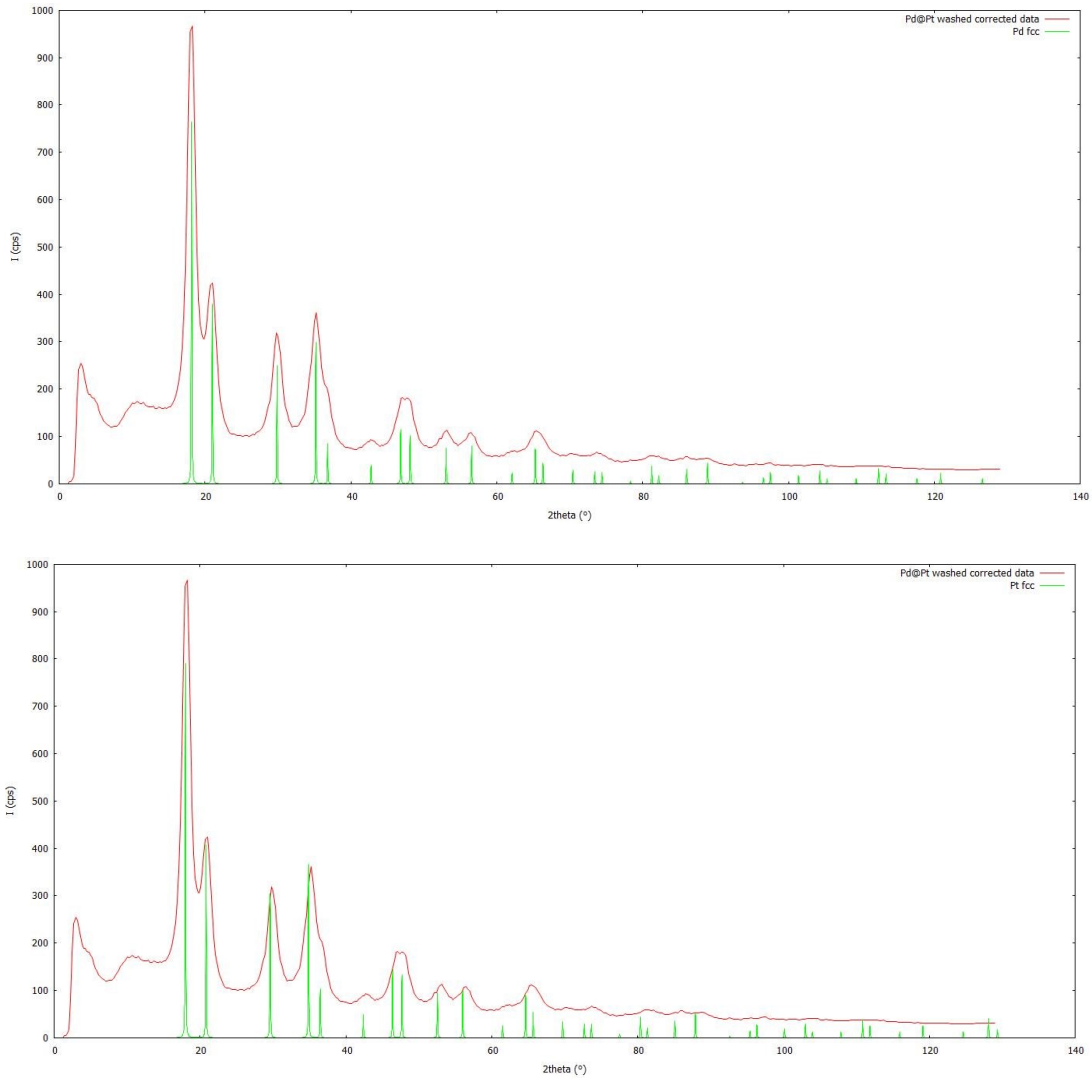

Figure S6. Comparison of WAXS patterns of the Pd@Pt colloid catalyst and pure Pd or pure Pt fcc structures

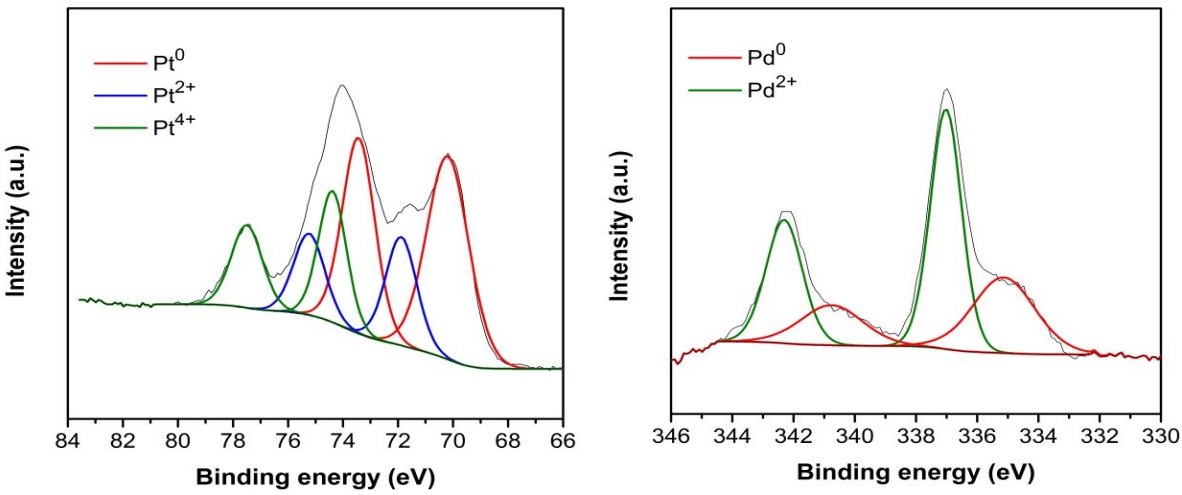

Figure S7. XPS spectra of Pd@Pt NPs showing Pt 4f and Pd 3d peaks.

The amount of surface Pt^0 and Pd^0 over Pd@Pt-PVP is 55% and 38%, respectively.

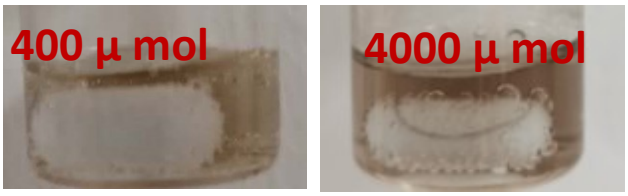

Figure S8. Picturesof the reaction mixture after CH_4 oxidation at 400 and 4000 µ mol H_2O_2.

Table S4. H_2O_2 consumption and gain factors of Pd, Pt, PtPd and Pd@Pt colloidal catalysts

Catalyst	Consumed H2O2 after 30 min reaction	Gain factor[a]
Pd	100%	0.011
PtPd	96%	0.013
Pd@Pt	82%	0.021
Pt	50%	0.0075

[a] Gain factor refers to the molar ratio between oxygenates produced and actual hydrogen peroxide consumed

Table S5. Scalability tests of the Pd@Pt colloid catalysts.

Total volume	Primary oxygenate produced (mol mol_{metal}^{-1})		Productivity (mol mol $_{metal}^{-1}$ h^{-1})
	CH_3OH	CH_3OOH	
2.4 ml	1.2	4.0	10.5
9.6 ml	1.7	1.8	7.1

The same reactor and same batch of catalysts were used. The total volume of the reactor is 30 ml.

Table S6. Remaining of H_2O_2 with varied reaction times using Pd@Pt colloidal catalyst

Reaction time	10 min	30 min	80 min
H_2O_2 remaining	36%	18%	10%

Table S7. Comparison of the catalytic performance obtained with Fe-based Fenton's type catalyst and Pd@Pt colloids nanocatalyst

Entry	Catalyst	Product amount (μmol)					Primary Oxygenated selectivity (%)
		CH_3OOH	CH_3OH	HCHO	HCOOH	CO_2	
1	Fe-Fenton[a]	1.2	0.1	0.15	0	0.17	77
2	Pd@Pt	2.3	4.4	0.3	0	0.18	92

[a] The Fe-Fenton system is prepared using $Fe(NO_3)_3 \cdot 9H_2O$ solution with the same amount of metal species as that for entry 2.

References

1. Z. Jin, L. Wang, E. Zuidema, K. Mondal, M. Zhang, J. Zhang, C. Wang, X. Meng, H. Yang, C. Mesters and F.-S. Xiao, *Science*, 2020, **367**, 193-197.
2. R. McVicker, N. Agarwal, S. J. Freakley, Q. He, S. Althahban, S. H. Taylor, C. J. Kiely and G. J. Hutchings, *Catal. Today*, 2020, **342**, 32-38.
3. C. Williams, J. H. Carter, N. F. Dummer, Y. K. Chow, D. J. Morgan, S. Yacob, P. Serna, D. J. Willock, R. J. Meyer, S. H. Taylor and G. J. Hutchings, *ACS Catal.*, 2018, **8**, 2567-2576.
4. Y. Kwon, T. Y. Kim, G. Kwon, J. Yi and H. Lee, *J. Am. Chem. Soc.*, 2017, **139**, 17694-17699.
5. J. Shan, M. Li, L. F. Allard, S. Lee and M. Flytzani-Stephanopoulos, *Nature*, 2017, **551**, 605-608.
6. S. Bai, F. Liu, B. Huang, F. Li, H. Lin, T. Wu, M. Sun, J. Wu, Q. Shao, Y. Xu and X. Huang, *Nat. Commun.*, 2020, **11**, 954.
7. Q. K. Shen, C. Y. Cao, R. K. Huang, L. Zhu, X. Zhou, Q. H. Zhang, L. Gu and W. G. Song, *Angew. Chem. Int. Edit.*, 2020, **59**, 1216-1219.
8. P. Xiao, Y. Wang, T. Nishitoba, J. N. Kondo and T. Yokoi, *Chem Commun (Camb)*, 2019, **55**, 2896-2899.
9. S. Bai, Y. Xu, P. Wang, Q. Shao and X. Huang, *ACS Catal.*, 2019, **9**, 6938-6944.
10. X. Cui, H. Li, Y. Wang, Y. Hu, L. Hua, H. Li, X. Han, Q. Liu, F. Yang, L. He, X. Chen, Q. Li, J. Xiao, D. Deng and X. Bao, *Chem*, 2018, **4**, 1902-1910.